Research Article | Vol. 30, No. 11 / 23 May 2022 / Optics Express 19974
Optics EXPRESS

General design method for dynamic freeform optics with variable functionality

SHOHREH SHADALOU* AND THOMAS J. SULESKI

Dept. of Physics & Optical Science, University of North Carolina Charlotte, Charlotte, NC 28223, USA
*sshadalo@uncc.edu

Abstract: We propose and demonstrate a general design method for refractive two-element systems enabling variable optical performance between two specified boundary conditions. Similar to the Alvarez lens, small, relative lateral shifts in opposite directions are applied to a pair of plano-freeform elements. The surface prescriptions of the boundary lenses and a maximum desired shift between freeform plates are the main design inputs. In contrast to previous approaches, this method is not limited to boundaries with similar optical functions and can enable a wide range of challenging, dynamic functions for both imaging and non-imaging applications. Background theory and design processes are presented both for cases that are conducive to analytical surface descriptions, as well as for non-analytic surfaces that must be described numerically. Multiple examples are presented to demonstrate the flexibility of the proposed method.

1. Introduction

Modern optical systems benefit from freeform surfaces that enable compact and high-performance designs by utilizing additional design freedoms without the constraint of rotational symmetry [1]. Optical designs with continuously variable properties, or so-called dynamic optics, can add new, desirable functionalities for a wide range of both imaging and non-imaging applications, including cameras, aberration generators, microscopy, optometry, lighting, beam shaping, AR/VR, medicine/dermatology, and lithography [2–11].

Early examples of optical systems with multiple functions include bifocal single-element lenses used for spectacles and later designs of single-element lenses with gradually changing optical power using surfaces defined by involute curves [12–14]. While interesting and beneficial, single elements of this type use only a portion of the clear aperture for each function.

Liquid lenses are another way to offer flexible functionality to an optical system by modulating lens curvature or refractive index. [15–21]. However, liquid lenses have potential drawbacks such as leakage, evaporation, manufacturing complexity, and performance instabilities. While zoom lens systems have been reported to enable continuously variable optical power and dynamic beam shaping [22–24], such systems usually involve multiple optics and require longitudinal movement of the components, which can result in larger system sizes.

Another type of dynamic lens system employs refractive lens pairs capable of generating continuously variable optical power by applying shifts in a transverse plane with respect to the optical axis. Early designs were based on the direct superposition concept in which the output wavefront can be considered as a superposition of individual wavefront deformations due to passing through each individual refractive plate. Examples using this approach generate adjustable optical power with two orthogonally shifted cylinder lenses with varying radii of curvature [25–27]. The individual elements were constructed as segments of a cone or involutes of a circle. This approach introduces distortion due to non-uniform optical power across the clear aperture and requires large lateral shifts that are undesirable in compact optical systems.

The next generation of dynamic optics was enabled using an integral method with pairs of plano-freeform refractive elements. By applying lateral relative shifts in opposite directions

#460078 https://doi.org/10.1364/OE.460078
Journal © 2022 Received 8 Apr 2022; revised 12 May 2022; accepted 13 May 2022; published 19 May 2022

Optics EXPRESS

to freeform pairs with matching surfaces, the output wavefront deformation can be related to the derivative of the individual freeform surfaces and the amount of applied shift [2,3,7,28]. Compared to the direct superposition approach described previously, the integration approach requires significantly smaller lateral shifts without introducing significant distortion. The Alvarez lens system is a well-known example of this approach that enables continuously tunable optical power [2]. Palusinski later extended the Alvarez concept to enable variable aberration generators [7]. The general form of these systems has a symmetrical working range with zero optical power P at no shift ($a = 0$) and inverse optical power at the same shifts in positive and negative directions, as shown in Fig. 1.

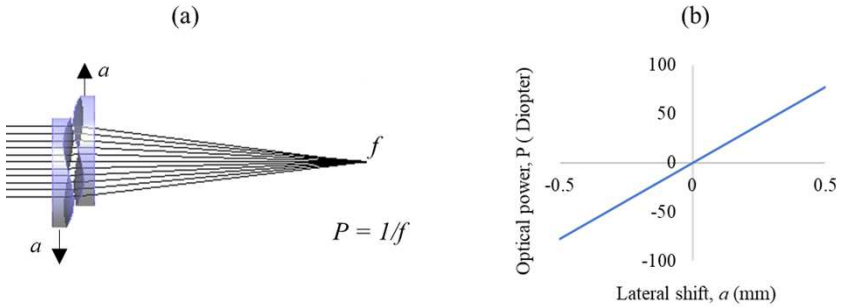

Fig. 1. (a) Schematic illustration of Alvarez lens system operation, (b) Optical power vs. lateral shift for a sample Alvarez lens system.

Researchers later proposed a simple design adjustment to shift the working range of the Alvarez lens to break the symmetric constraint and enable optical power at zero relative shift ($a = 0$) [29]. However, breaking the symmetric constraint becomes more difficult when other dynamic optical properties are considered. Researchers recently reported dynamic beam shaping elements based on the Alvarez concept that transform a Gaussian input beam into uniform irradiance outputs of different sizes with optical power at zero relative shift [30–33]. Although the reported results are very promising, the method requires multiple intermediate static designs and curve fits that can be time-consuming, and the target size is assumed to change linearly with lateral shifts of the freeform plates, which may not always be the case. Defining target patterns in advance is challenging for cases having non-linear relations between shift and target size.

Previous design approaches for dynamic freeform optics have also been limited to optical composites with similar functions along the shifting range of the freeform elements. For example, the Alvarez lens enables variable spherical power, and adjustable aberration generators vary a specific aberration along the working range. In contrast, consider an optical system working between non-similar optical conditions, such as a novel beam-shaping system capable of dynamically changing the output from a circle to a square. In addition, modern non-imaging designs can heavily utilize freeform surfaces obtained by numerical design approaches for compact, efficient optical systems [34–46]. The resulting surfaces are usually described by point clouds rather than equations. Variable illumination modes have been previously enabled by switching optical components [47,48]; However, designing dynamic systems to enable continuously variable optical performance for these types of systems is challenging and not been addressed by previous design methods.

In this paper, we extrapolate the previously reported approach for dynamic beam shaping [30–33] to form a generalized design method capable of varying optical performance between two arbitrary boundary conditions. This method eliminates the needs for intermediate designs and symmetrical constraints in the working range required by previous approaches. In addition, this method can be applied to surfaces described analytically by equations or numerically through

Optics EXPRESS

point clouds. The resulting designs can be used directly in optical systems or considered as starting points for further optimizations using optical software based on the required accuracy and performance. The proposed method enables novel optical concepts for both imaging and non-imaging applications.

Section 2 presents a detailed overview of the proposed design method. Sections 3 and 4 demonstrate and verify the general design method with simulation results for both analytical and numerical design examples, followed by conclusions in Section 5.

2. General design method for dynamic freeform optics

The proposed general technique combines the superposition and integration approaches outlined in Section 1 to speed up and facilitate complex designs. Thin lens approximations and no air gap between the freeform pairs are assumed in theory. The optical material is the same for both boundary elements and the resulting freeform plates, but different materials may be used if the respective refractive indices are considered. To simplify the calculations, the thickness variation parameter illustrated in Fig. 2 as *T(x, y)*, has been used [7].

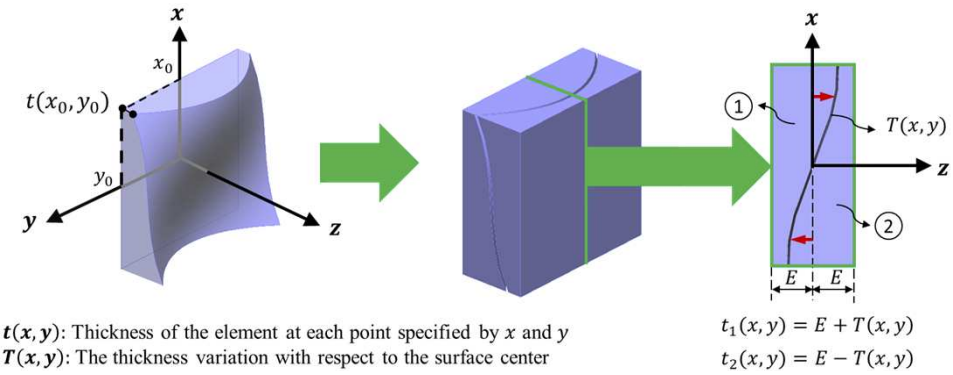

Fig. 2. Illustrating the geometrical thickness and thickness variation of a double refractive element.

The key inputs for the proposed method are two static designs representing the performance boundaries, and the maximum lateral shift value (a_{max}) between the freeform pairs. The integration technique can be used to construct a dynamic system with plano-freeform plates if static boundary elements have inverse optical thicknesses. As presented by Palusinski *et al.* in [7], the optical path difference concept can be used to calculate the wavefront deformation of a collimated beam passing through the shifting plates. The same notation is used here to avoid confusion. The optical path difference imposed by each plate is:

$$OPD(x, y) = (n - 1)T(x, y), \tag{1}$$

where n is the refractive index, *T(x, y)* is the thicknesses variation, and x and y are transverse coordinates across the plane perpendicular to the optical axis, as shown in Fig. 2.

When two lenses with inverse optical thicknesses are each laterally displaced by distance a in opposite directions along the x axis, as shown in Fig. 3, the resulting wavefront deformation is given by:

$$W(x, y) = (n - 1)[T(x + a, y) - T(x - a, y)]. \tag{2}$$

The wavefront deformation can be rewritten and simplified as follows:

$$W(x, y) = 2a(n - 1)\frac{[T(x + a, y) - T(x - a, y)]}{2a} \approx 2a(n - 1)\frac{\partial T(x, y)}{\partial x}. \tag{3}$$

Optics EXPRESS

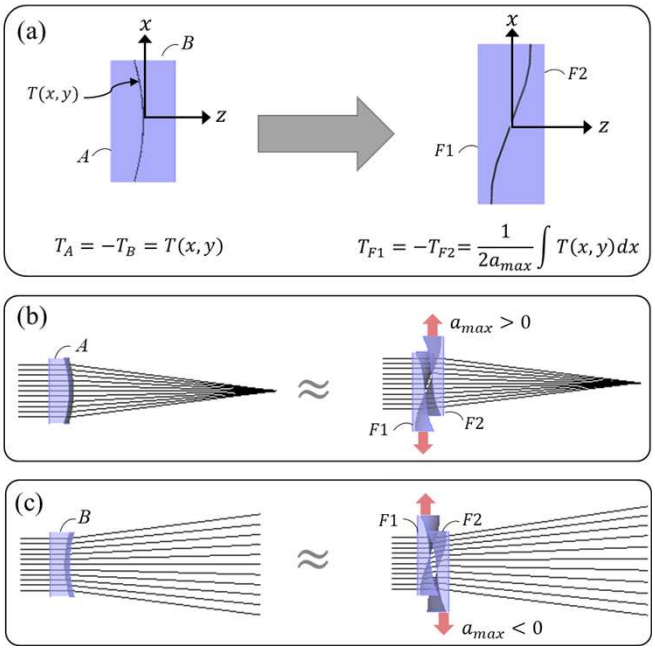

Fig. 3. (a) Design of dynamic freeforms from boundary elements with inverse thickness variation. For an example Alvarez lens, ray tracing through (b) first boundary element and dynamic system at maximum positive shift, and (c) second boundary element and dynamic system as maximum negative shift.

The effective composite optical thickness of the two plates is thus given by:

$$T_C(x, y) \approx 2a \frac{\partial T(x, y)}{\partial x}. \tag{4}$$

Equation (4) relates the composite optical thickness of two refractive plates with inverse surfaces to the relative lateral shifts between them and the derivative of the optical thickness variation. For design, the inverse problem starts from the composite optical thicknesses with maximum shift values applied and derives through integration the required optical thicknesses of the freeform elements needed for dynamic functionality. In the case of the simple Alvarez lens, then the composite thickness is $2\beta a(x^2 + y^2)$ and the thickness variation is $\beta(x^3/3 + xy^2)$. A tilt term can be added to the thickness variation as $\beta(x^3/3 + xy^2)+Dx$, where D is a weighting coefficient, to minimize the thickness of the freeform plates without impacting the calculations [2,7].

The design approach described in [30–33] for dynamic beam shaping considers cases in which the two boundaries do not have matching thicknesses but do have comparable functions and surface prescriptions, and identifying intermediate static designs is possible. In this paper we generalize existing methodologies to enable rapid dynamic designs that work between two arbitrary optical conditions without the need for intermediate static designs.

To derive general formulas for dynamic freeform pairs, we first consider thickness variations of two boundary elements $T_A(x, y)$ and $T_B(x, y)$ with no matching constraints. These two boundaries are transformed into two intermediate elements using the average thickness variation, as illustrated in Fig. 4. The thicknesses variation of the new elements, $T_{A'}(x, y)$ and $T_{B'}(x, y)$, are then calculated as follows:

$$T_{A'} = T_A - T_{avg} = T_A - \frac{(T_A + T_B)}{2} = +\frac{(T_A - T_B)}{2}, \tag{5}$$

Optics EXPRESS

$$T_{B'} = T_B - T_{avg} = T_B - \frac{(T_A + T_B)}{2} = -\frac{(T_A - T_B)}{2}. \tag{6}$$

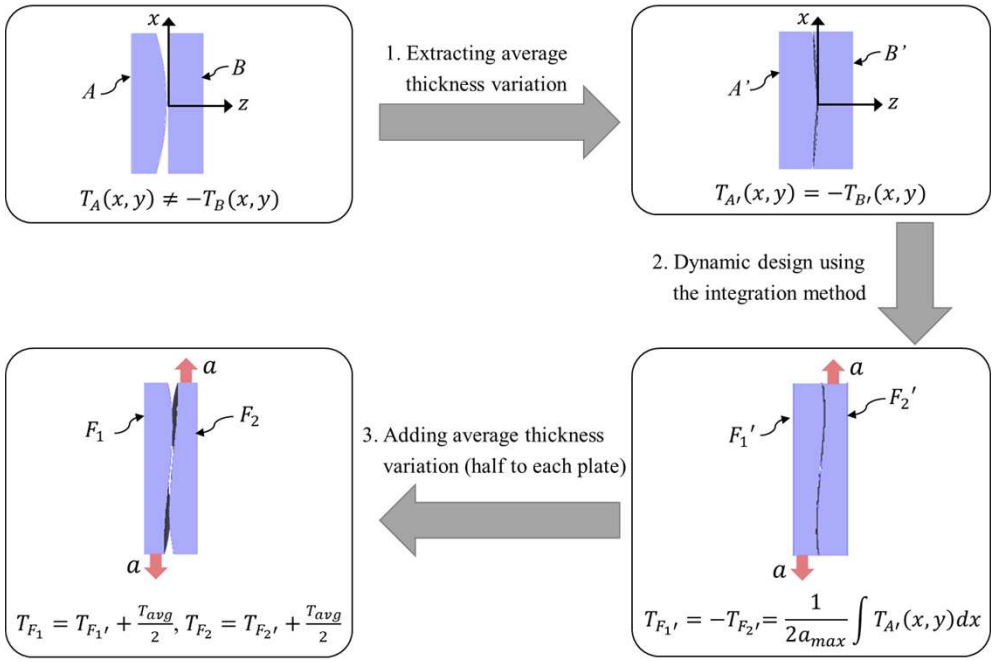

Fig. 4. Moving from arbitrary static boundary designs to dynamic dual element system using proposed method.

Equations (5), (6) show that the 'new' boundary elements have inverse thickness variations, and thus the design problem can be solved using the integration approach discussed previously. Thus, variable optical properties changing from $T_{A'}$ to $T_{B'}$ are achieved as opposite lateral shifts are applied to a pair of freeform plates with the following optical thicknesses:

$$T_{F1'} = -T_{F2'} = \frac{1}{2a_{\max}} \int T_{A'} dx = \frac{1}{2a_{\max}} \int \frac{T_A - T_B}{2} dx, \tag{7}$$

where a_{max} is the magnitude of the maximum lateral shift applied to each dynamic plate in opposite directions.

Finally, to transform back to the original design problem varying from $T_A(x, y)$ to $T_B(x, y)$, the direct superposition concept is applied to add the initially extracted average optical thickness back to the system. Therefore, the final optical thicknesses of the dynamic freeform plates are given as follows:

$$T_{F1} = T_{F1'} + \frac{T_{avg}}{2} + Dx = +\frac{1}{2a_{\max}} \int \frac{T_A - T_B}{2} dx + \frac{T_A + T_B}{4} + Dx, \tag{8}$$

$$T_{F2} = T_{F2'} + \frac{T_{avg}}{2} - Dx = -\frac{1}{2a_{\max}} \int \frac{T_A - T_B}{2} dx + \frac{T_A + T_B}{4} - Dx, \tag{9}$$

where the Dx tilt term is added to minimize the thicknesses of the dynamic freeform plates. The overall design process is illustrated graphically in Fig. 4.

Optics EXPRESS

As a test, we apply the maximum shift a_{max} to the dynamic freeform plates and check the output wavefront as a superposition of wavefront deformations induced by each plate:

$$\begin{aligned} W(x,y) &= (n-1)[T_{F1}(x+a_{\max},y) + T_{F2}(x-a_{\max},y)] \\ &= (n-1)\left[\frac{1}{2a_{\max}}\int \frac{T_A(x+a_{\max},y)-T_B(x+a_{\max},y)}{2}dx + \frac{T_A(x+a_{\max},y)+T_B(x+a_{\max},y)}{4}\right. \\ &\quad \left. -\frac{1}{2a_{\max}}\int \frac{T_A(x-a_{\max},y)-T_B(x-a_{\max},y)}{2}dx + \frac{T_A(x-a_{\max},y)+T_B(x-a_{\max},y)}{4}\right] \\ &= (n-1)\left[\frac{1}{2}\int \frac{T_A(x+a_{\max},y)-T_A(x-a_{\max},y)}{2a}dx - \frac{1}{2}\int \frac{T_B(x+a_{\max},y)-T_B(x-a_{\max},y)}{2a}dx\right. \\ &\quad \left. +\frac{T_A(x+a_{\max},y)+T_A(x-a_{\max},y)}{4} + \frac{T_B(x+a_{\max},y)+T_B(x-a_{\max},y)}{4}\right] \\ &\approx (n-1)\left[\frac{T_A(x,y)}{2} - \frac{T_B(x,y)}{2} + \frac{T_A(x,y)}{2} + \frac{T_B(x,y)}{2}\right] \approx (n-1)T_A(x,y) \approx W_A(x,y). \end{aligned} \tag{10}$$

Thus, within the assumed approximations of thin-phase and zero-air gap, a maximum relative shift in one direction creates the wavefront deformation of the first optical boundary condition, $W_A(x, y)$. Analogous calculations for the maximum shift in the opposite direction creates the wavefront deformation of the second optical boundary condition, $W_B(x, y)$.

While determining the exact error and optimizing the dynamic system for non-zero thickness is more involved, optical design software can be used for further optimization to minimize the errors based on the accuracy required in various applications. Similarly, the physical distance between dynamic freeform pairs was neglected to simplify the calculations. To decrease this air gap in real designs and to simplify optic manufacturing by lowering the surface depth modulation, it is recommended to include a tilt factor in both freeform surfaces as discussed previously. We note that the proposed design method may produce equivalent or dissimilar freeform plates depending on the two boundary designs as presented in Eqs. (8), (9). Finding a tilt factor that minimizes the sag is straightforward in the case of identical plates, but we recommend choosing a tilt factor that minimizes both surface depth modulations concurrently for dissimilar plates.

While the processes and derivations discussed above are analytical in nature, the proposed design methodology can be implemented either analytically or numerically. The analytical approach is the logical choice if the boundary elements are readily defined by surface equations that can be integrated analytically. However, if the boundary elements are produced numerically and specified in point clouds, a numerical implementation of the same procedures is desirable alternative since it eliminates the need for curve fitting the surfaces of the boundary elements. Numerical methods are also advantageous when boundary surface equations are provided but the integration of their difference is challenging or the acquired solution for the dynamic plates is difficult to create analytically in optical software. However, further optimization of numerical freeform surfaces may be more difficult. Both analytical and numerical implementations are discussed and demonstrated in greater detail in the following sections using multiple design examples.

3. Analytical design examples for dynamic freeform optics

In this section, the analytical implementation of the proposed general design method is demonstrated through several examples. We assumed that the boundary elements and their corresponding dynamic freeforms are constructed of identical materials. After definition of the design parameters and boundary elements for each example, the thickness variations for the dynamic freeform plates are computed using the method of Section 2. The thickness variations can be related to surface profiles to model the optical elements in optical software. To ease the manufacturing process and allow for smaller air gaps between freeform plates, the surface modulations are reduced by applying the same linear tilt factor to each of the freeform surface equations. To ensure the same clear aperture as the boundary elements in a dynamic system, an additional section equal to the overall shift range must be added to each freeform plate, as illustrated in Fig. 5.

Optics EXPRESS

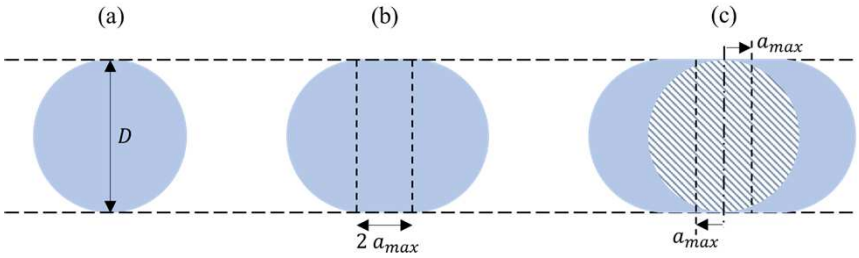

Fig. 5. (a) Aperture geometry of a circular boundary element, and (b, c) corresponding aperture geometry of resulting dynamic plates.

The first example demonstrates variable positive spherical optical power, the second illustrates variable cylindrical power, and the final example generates a uniform circular irradiance pattern from a Gaussian He-Ne laser and smoothly converts it to a uniform square-shaped irradiance pattern. As discussed previously, the proposed method requires two static boundary designs and the maximum lateral shift of dynamic freeform plates as the main inputs. The design process and simulation results are presented for each example. The first two cases are simulated in LightTools and the third is evaluated in VirtualLab Fusion.

3.1. Analytical example 1: Variable positive-spherical power lens system

For this example, we assumed polycarbonate ($n = 1.59$) as the design material and a 550 nm design wavelength. The boundary elements have circular apertures with 4 mm diameters and 0.75 mm thicknesses. Unlike the traditional Alvarez lens, this design has positive power at $a = 0$ and for all values. Table 1 lists the input parameters and the resulting freeform surfaces calculated using Eqs. (8), (9). The linear tilt term in the freeform plates is calculated using MATLAB to minimize the overall sag along the freeform surfaces.

Table 1. Primary inputs and outputs of variable positive-power lens system example

Main inputs	First boundary element	Flat with zero optical power, $T_A(x, y) = 0$, $P_A = 0$
	Second boundary element	$T_B(x, y) = -0.05(x^2 + y^2)$, $P_B = 61$ *Diopter*
	Lateral shift range	$-0.4 < a < +0.4$ *mm*
Main outputs	First freeform plate	$T_{F1}(x, y) = 0.03125(\frac{x^3}{3} + xy^2) - 0.0125(x^2 + y^2) - 0.0743x$
	Second freeform plate	$T_{F2}(x, y) = -0.03125(\frac{x^3}{3} + xy^2) - 0.0125(x^2 + y^2) + 0.0743x$

The boundary lenses and resulting dynamic design were modeled using LightTools, as illustrated in Fig. 6. A 100 µm air gap was set between the freeform plates to ensure that they do not contact during shifting. The dynamic freeform pair delivers variable positive optical power (and focal length) between the boundary values, as shown in Fig. 7 and Visualization 1.

3.2. Analytical example 2: Variable cylindrical lens system

The second design example demonstrates a variable cylindrical lens system using the proposed design method. The same general configuration and design parameters as in the first example are used here, but with different boundary element surface equations and dynamic freeform shift range, as shown in Table 2. As before, the equations of the dynamic freeform surfaces are calculated using Eqs. (8), (9) and a linear tilt term added to reduce the depth modulation.

LightTools was again used to model boundary elements irradiated by a uniform disc source with a diameter of 3 mm. Figure 8 shows the output irradiances of the simulated boundary

Optics EXPRESS

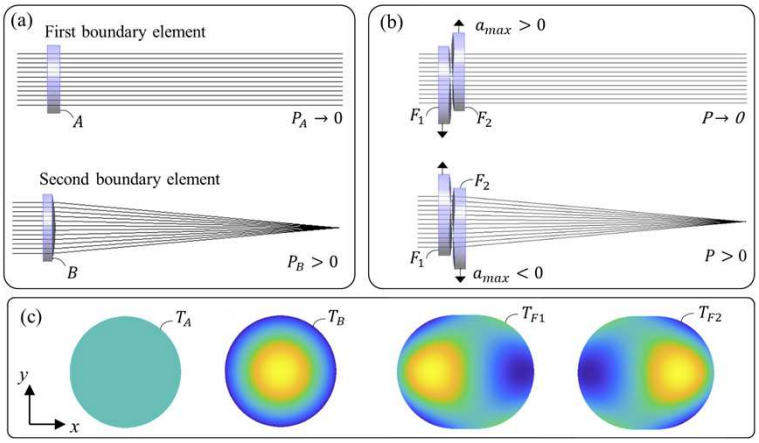

Fig. 6. Ray traces for (a) boundary elements vs. (b) dynamic freeform plates with maximum lateral shifts applied for first analytical design example, and (c) thickness variations of boundary and dynamic freeform elements.

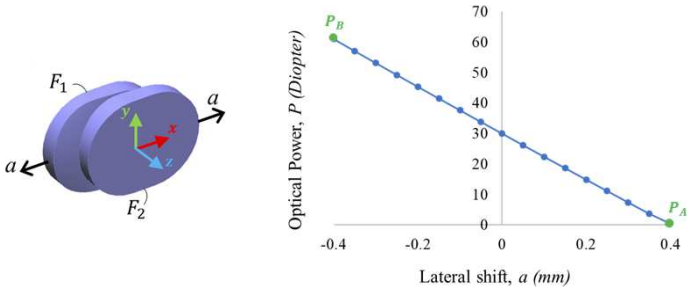

Fig. 7. Optical power vs. lateral shift for variable positive-power lens system.

Table 2. Primary inputs and outputs of variable cylindrical lens system example

Main inputs	First boundary element	$T_A(x, y) = -0.04x^2$
	Second boundary element	$T_B(x, y) = -0.04y^2$
	Lateral shift range	$-0.5 < a < +0.5$ mm
Main outputs	First freeform plate	$T_{F1}(x, y) = +0.02(xy^2 - \frac{x^3}{3}) - 0.01(x^2 + y^2) + 0.0084x$
	Second freeform plate	$T_{F2}(x, y) = -0.02(xy^2 - \frac{x^3}{3}) - 0.01(x^2 + y^2) - 0.0084x$

elements at 1 m distance. Figure 9 and Visualization 2 illustrate the change of output irradiance with various shifts between the freeform plates.

3.3. *Analytical example 3: Circular to square dynamic beam shaper*

This design example develops a dynamic beam shaper that converts a circular Gaussian input beam from a uniform circular output pattern to a uniform square output pattern. Static designs of circular and square beam shapers presented in [49] were used to accelerate the design process. As illustrated in Fig. 10, the first boundary element produces a uniform circular distribution, and the second boundary element delivers a square shape of irradiance output from a Gaussian incident beam. Table 3 lists the design parameters. The analytical design equations for each boundary element are presented in Supplement 1.

Optics EXPRESS

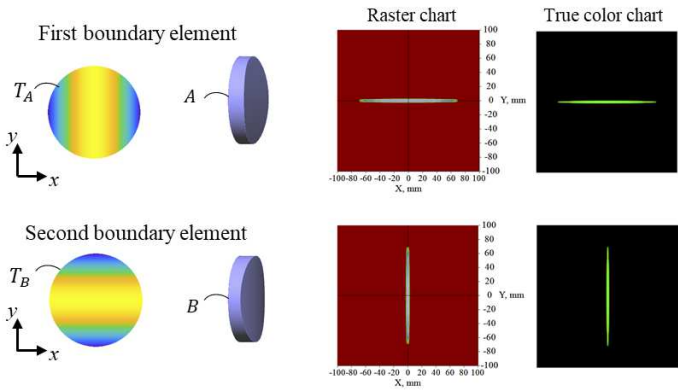

Fig. 8. Irradiance patterns at 1 m distance from a uniform collimated disc source after the boundary elements of second analytical design example.

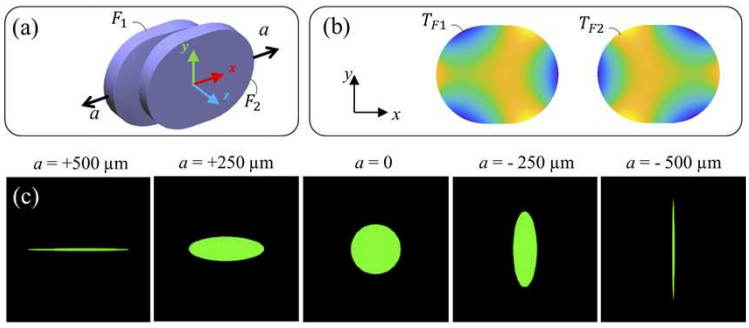

Fig. 9. (a, b) Freeform surfaces, and (c) irradiance patterns at 1 m distance from a uniform collimated disc source after passing the tunable cylindrical-power lens system at different lateral shifts.

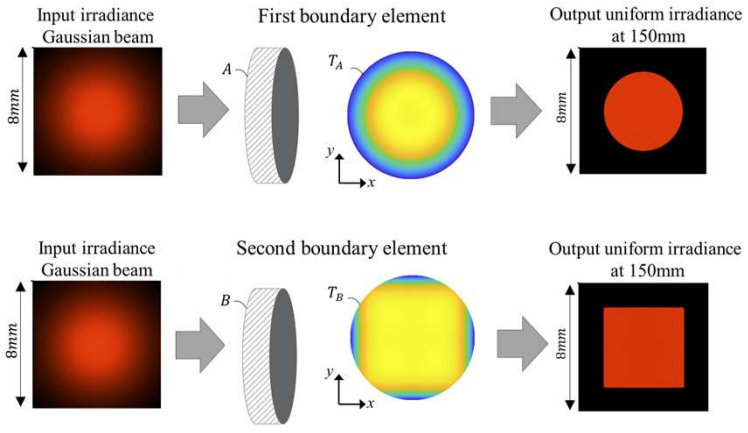

Fig. 10. Boundary elements of the third analytical design example.

Optics EXPRESS

Table 3. Input design parameters for dynamic beam shaper example

Wavelength	632.8 nm
Input beam waist diameter	6 mm
Material (index)	PMMA (n =1.49)
Target distance	150 mm
Boundary element diameters	12 mm
Boundary element thicknesses	2 mm
First boundary output beam diameter	5 mm
Second boundary output beam square side	5 mm
Lateral shift range of freeform pair	$-300 < a < +300$ µm

As before, the surface profiles of the dynamic freeform plates are computed by Eqs. (8), (9) using the boundary element profiles and maximum shift range. The resulting freeform surface equations are presented in Supplement 1. The resulting coefficients were then used to model the dynamic freeform system in VirtualLab Fusion. as shown in Fig. 11. The surfaces in this design example are much more complex than the first two cases, illustrating the power and flexibility of the proposed general design method.

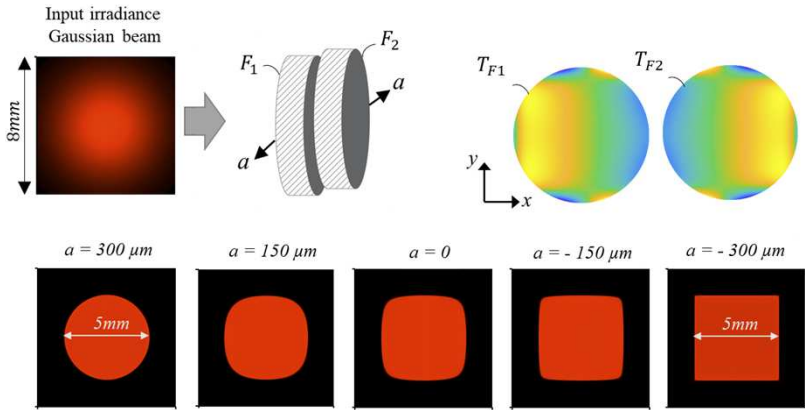

Fig. 11. Freeform surface geometries and simulated output irradiance patterns at 150 mm distance from dynamic-pattern beam shaper on an 8-by-8 mm detector.

4. Numerical design examples for dynamic freeform optics

As discussed in Section 2, the general dynamic design method we propose can also be implemented numerically for surfaces that are not conducive to analytical descriptions. The height maps of boundary elements are represented as thickness variations, $T_A(x, y)$ and $T_B(x, y)$ using point clouds for the calculation of the dynamic freeform pairs using Eqs. (8), (9) and numerical integration methods. We note that, in the default numerical implementation, the sizes of the dynamic plates will be the same as the boundary elements. Therefore, it may be useful to consider larger boundary lenses if they are equation based, or to limit the aperture size in the dynamic system to ensure rays are passing through both freeform plates and have proper functionality. The maximum possible shift can be set initially based on the size of the boundary elements and then modified during the design process as the optical performance of the dynamic system is evaluated.

Optics EXPRESS

The trapezoidal rule is a common method of performing numerical integration [50]. We developed a custom MATLAB code to accelerate the design process. To simplify the calculations, we reduced the integration dimension from 3D to 2D by discretizing the function along the Y axis and moving from XYZ space to XZ planes, as illustrated in Fig. 12. The cumulative integration for x with respect to zero was used at each XZ plane using the MATLAB "Cumtrapz" function. The accuracy of the numerical integration can be improved by increasing the number of surface points, but at the cost of increased computation time.

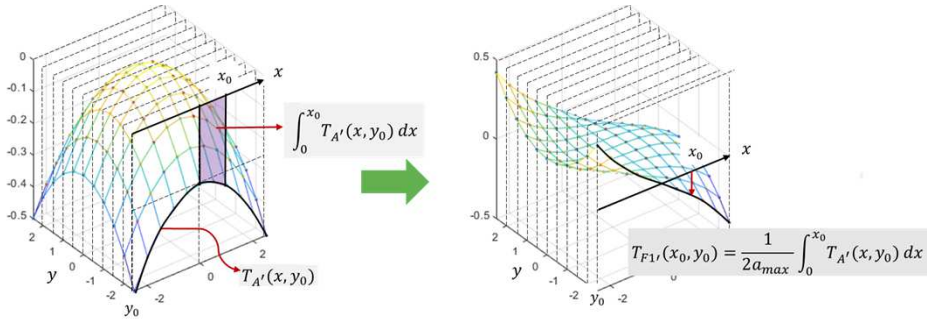

Fig. 12. Numerical integration approach applying the trapezoidal rule for proposed freeform design method.

In this section we present three design examples solved using numerical methods. In the first example, we repeat the design of the variable positive-spherical power lens system from Section 3 using the numerical method and compare the outcomes. The second example considers a square to hexagonal dynamic pattern generator. The third example demonstrates the flexibility of the general approach through a dynamic pattern generator that we believe would be impractical (or impossible) to implement with currently available analytical methods.

4.1. Numerical example 1: Variable positive-spherical power lens system

The boundary lenses for this design example are built from the first analytical example, as listed in Table 1. The point clouds of boundary lenses were generated in MATLAB with 0.05 mm resolution. By taking the thickness variation of the surface points and a maximum shift of 0.4 mm, dynamic freeform surface points were numerically generated in MATLAB using Eqs. (8), (9). We utilized the numerical integration approach discussed above. The MATLAB code was linked to LightTools to speed up analysis of the system'ptical performance. Figure 13 illustrates construction of the desired freeform plate geometry in LightTools to match the geometry of the first analytical example.

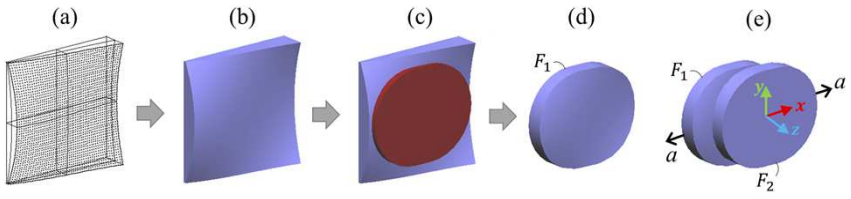

Fig. 13. (a) Constructing the freeform base plate in LightTools from MATLAB point cloud; (b) 3D model of freeform base, (c) intersecting freeform base with desired aperture geometry, (d) freeform plate with desired oval-shaped geometry, (e) 3D model of dynamic freeform system for first numerical example.

Optics EXPRESS

The optical power of the dynamic system was determined as the inverse of the back focal length at different lateral shifts using a parameter analyzer in LightTools. The results obtained are in excellent agreement with the analytic results shown in Fig. 7. Table 4 compares the values obtained using the analytic and numerical approaches. The differences increase slightly as the lateral shift is increased from zero to the maximum positive shift. In the case of maximum positive shift, the focal point expands to infinity, making the system extremely sensitive to lateral shift and resulting in a larger difference.

Table 4. Optical power vs lateral shift for variable positive-power lens system

Lateral shift, *a (mm)* / Design method	0.399[a]	0.3	0.2	0.1	0	−0.1	−0.2	−0.3	−0.4
Power-Analytic (Diopters)	0.51	7.4	14.8	22.4	29.9	37.6	45.3	53.1	61.0
Power-Numerical (Diopters)	0.52	7.6	15.0	22.6	30.2	37.8	45.6	53.4	61.4
% Difference	1.9	2.7	1.3	0.9	0.7	0.7	0.6	0.6	0.7

[a]The focal point at 0.4 mm lateral shift goes to infinity, so we considered a slightly smaller shift value

4.2. *Numerical example 2: Simple dynamic pattern generator*

Different numerical approaches to designing freeform lenses that allows for the generation of prescribed light distributions in illumination systems have recently been reviewed in the literature [34]. Recent advances in optical software also facilitate the numerically design of refractive elements to map the input light to a prescribed output light distribution. To this end, we used the LightTools Freeform Design module to create the boundary elements needed for this design example assuming the uniform plane wave source. In this example, we demonstrate the proposed numerical design method for a dynamic pattern generator changing the irradiance distribution between square and hexagonal target patterns.

The mesh grids of the resulting freeform surfaces were adjusted to uniform XY grids for compatibility with custom MATLAB code developed to calculate the thickness variations of dynamic freeform plates. The boundary elements are 5×5 mm with 0.75 mm thickness and a 4×4 mm uniform source. The design material and design wavelength are PMMA and 550 nm, respectively. The two boundary elements constructed in LightTools and the resulting illumination patterns 2 m from the first element interface are shown in Fig. 14.

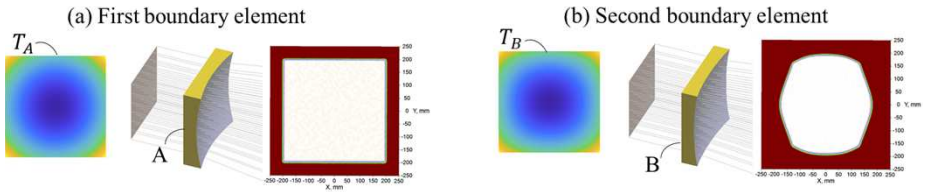

Fig. 14. Boundary elements of dynamic pattern generator producing (a) square, and (b) hexagonal patterns.

As in the previous example, the MATLAB code was linked to LightTools to import the surface height maps from the two boundary elements to accelerate the dynamic design process. Dynamic freeform point clouds were numerically calculated in MATLAB considering 200 by 200 mesh grids over the 5×5 mm mesh extent following Eqs. (8), (9) with a maximum shift of 0.2 mm. The resulting points were transferred to LightTools for optical performance evaluation as illustrated in Fig. 15 and Visualization 3. The aperture size and thicknesses of the freeform plates were

Optics EXPRESS

assumed to be the same as the boundary elements. A 500 μm air gap was set between the freeform plates to avoid collision during shifting.

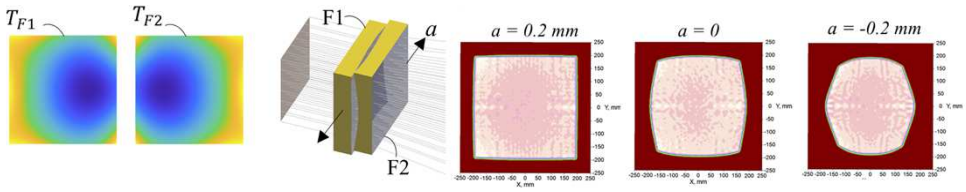

Fig. 15. Dynamic pattern generator varying from square to hexagonal pattern with applied lateral shift.

4.3. *Numerical example 3: Complex dynamic pattern generator*

The results obtained from the previous example could arguably be achieved using analytic representations of the target patterns. For this reason, we repeated the process with the same design parameters but for significantly more complex target patterns that are not feasible to represent in analytic form. The two boundary elements were again constructed using the LightTools Freeform Design module assuming uniform plane wave sources. The target patterns and resulting illumination patterns are shown in Fig. 16. The resulting dynamic system performance between the two boundaries is shown in Fig. 17 and Visualization 4. These results demonstrate the utility of the proposed general design method for dynamic freeform optical systems and show the potential for novel applications.

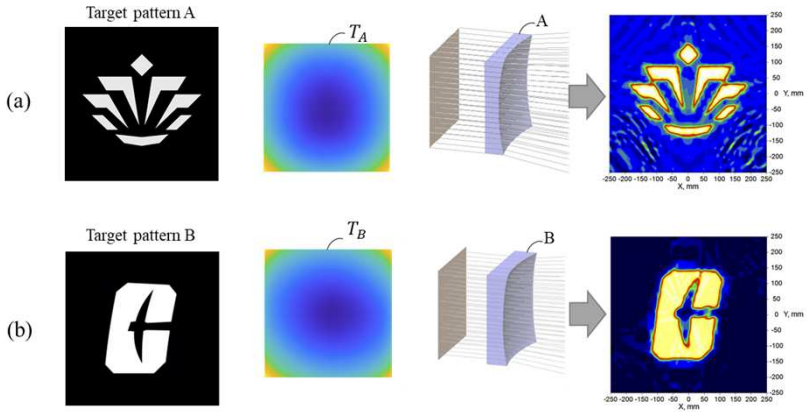

Fig. 16. (a) First and (b) second boundary elements and performance for complex illumination patterns.

Optics EXPRESS

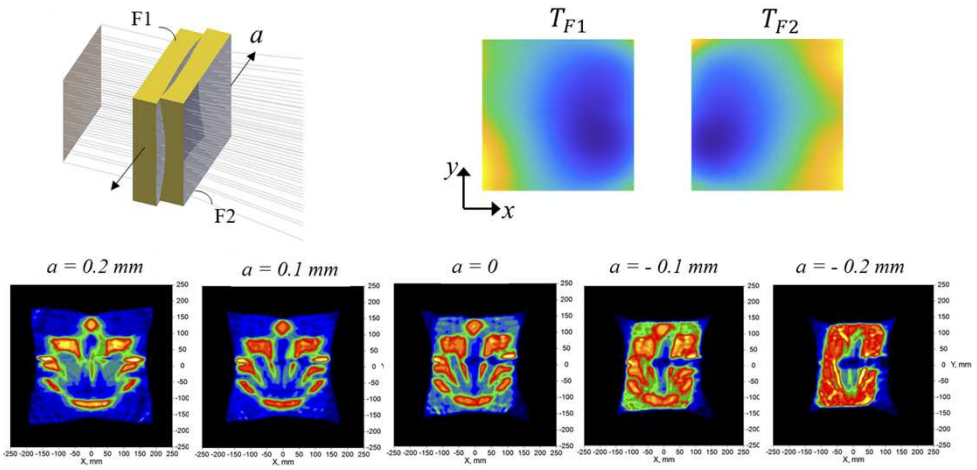

Fig. 17. Dynamic pattern generator varying between two complex illumination patterns with applied lateral shift.

5. Conclusions

We have presented accessible dynamic freeform design techniques for refractive two-element system that allows for varying optical performance between two defined boundary conditions. Similar to the Alvarez lens, pairs of plano-freeform elements are subjected to small, relative lateral shifts in opposing directions. The surface prescriptions of the boundary lenses, as well as the maximum desired shift between freeform plates, serve as the primary design inputs. This approach has advantages over prior methods in that it is not restricted to boundaries with similar optical functions and may be used to create a broad variety of challenging dynamic functions for both imaging and non-imaging applications. Depending on the characteristics of the boundary elements, this generalized technique can be implemented analytically or numerically. The analytical method is preferable if the boundary elements are easily specified using integrable surface equations without the need for surface fitting. Numerical approaches are useful when surface fitting would otherwise be required, and when boundary surface equations are available but problematic to integrated or to otherwise implement in optical software.

This general method was investigated and validated through multiple analytical and numerical design examples. The dynamic freeform systems utilized in the design examples were computed in MATLAB using the general formula reported in this paper and their optical performance was determined using commercial optical design tools. The simulation results for all design examples are quite promising, even though no additional optical system adjustments or optimizations were performed. We note that that the dynamic beam shaper example designed using the analytical approach and the dynamic pattern generator designed using the numerical approach would be difficult or impossible to create with previously available design approaches, demonstrating the utility of the proposed method.

Funding. National Science Foundation I/UCRC Center for Freeform Optics (IIP-1822026, IIP-1822049).

Acknowledgments. The authors would like to thank Synopsys for providing the LightTools license. We would also like to acknowledge useful discussions with Dr. William Cassarly at Synopsys and Dr. Christoph Menke from Carl Zeiss AG.

Disclosures. The authors declare no conflicts of interest.

Data availability. Data underlying the results presented in this paper are not publicly available at this time but may be obtained from the authors upon reasonable request.

Optics EXPRESS

Supplemental document. See Supplement 1 for supporting content.

References

1. J. P. Rolland, M. A. Davies, T. J. Suleski, C. Evans, A. Bauer, J. C. Lambropoulos, and K. Falaggis, "Freeform optics for imaging," Optica **8**(2), 161–176 (2021).
2. L. W. Alvarez and W. E. Humphrey, "Variable-power lens and system," U.S. patent 3,507,565A (21 April 1970).
3. J. G. Baker, "Variable power, analytic function, optical component in the form of a pair of laterally adjustable plates having shaped surfaces, and optical systems including such components," U.S. patent 3,583,790 (8 June 1971).
4. N. Matsuura, M. Kanno, H. Takeuchi, and A. Ishikawa, "Endoscope with variable illumination angle," U.S. patent 4,736,734 (12 April 1988).
5. L. Kleinburg and M. J. Danley, "Variable shutter illumination system for microscope," U.S. Patent 5,299,053 (29 March 1994).
6. S. S. Rege, T. S. Tkaczyk, and M. R. Descour, "Application of the Alvarez-Humphrey concept to the design of a miniaturized scanning microscope," Opt. Express **12**(12), 2574–2588 (2004).
7. I. A. Palusinski, J. M. Sasián, and J. E. Greivenkamp, "Lateral-shift variable aberration generators," Appl. Opt. **38**(1), 86–90 (1999).
8. S. Moein and T. J. Suleski, "Freeform optics for variable extended depth of field imaging," Opt. Express **29**(24), 40524–40537 (2021).
9. J. Koerber, G. D. Boreman, and T. J. Suleski, "Broadband Variable Transmission Sphere for Fizeau Interferometry," Optics **3**(1), 88–98 (2022).
10. A. Wilson and H. Hua, "Design and demonstration of a vari-focal optical see-through head-mounted display using freeform Alvarez lenses," Opt. Express **27**(11), 15627–15637 (2019).
11. S. Shadalou, W. J. Cassarly, and T. J. Suleski, "Tunable illumination for LED-based systems using refractive freeform arrays," Opt. Express **29**(22), 35755–35764 (2021).
12. A. G. Poullain and D. H. J. Cornet, "Optical lens," U.S. patent 1,143,316 (15 June 1915).
13. H. J. Birchall, "Lens of variable focal power having surfaces of involute form," U.S. patent 2,475,275 (5 July 1949).
14. E. C. Ernest, "Spectacle lens," U.S. patent 2,109,474 (1 March 1938).
15. D. Y. Zhang, V. Lien, Y. Berdichevsky, J. Choi, and Y. H. Lo, "Fluidic adaptive lens with high focal length tunability," Appl. Phys. Lett. **82**(19), 3171–3172 (2003).
16. H. Ren and S. T. Wu, "Variable-focus liquid lens," Opt. Express **15**(10), 5931–5936 (2007).
17. N. T. Nguyen, "Micro-optofluidic Lenses: A review," Biomicrofluidics **4**(3), 031501 (2010).
18. B. Berge and J. Peseux, "Variable focal lens controlled by an external voltage: An application of electrowetting," Eur. Phys. J. E **3**(2), 159–163 (2000).
19. S. Sato, "Liquid-crystal lens-cells with variable focal length," Jpn. J. Appl. Phys. **18**(9), 1679–1684 (1979).
20. M. Ye and S. Sato, "Optical properties of liquid crystal lens of any size," Jpn. J. Appl. Phys. **41**(Part 2, No. 5B), L571–L573 (2002).
21. H. C. Lin, M. S. Chen, and Y. H. Lin, "A review of electrically tunable focusing liquid crystal lenses," Trans. Electr. Electron. Mater. **12**(6), 234–240 (2011).
22. E. I. Betensky, J. B. Caldwell, I. A. Neil, and T. Yamanashi, "Zoom lens system," U. S. patent 6,961,188 B2 (1 Nov. 2005).
23. T. Yamanashi, "Wide angle zoom lens," U. S. 8,503,102 B2 (6 Aug. 2013).
24. W. Li, S. Wei, Z. Fan, Z. Zhu, and D. Ma, "Variable-diameter beam-shaping system design with high zoom ratio containing aspheric optical components," Appl. Opt. **60**(3), 705–713 (2021).
25. I. Kitajima, "Improvements in lenses," U. K. patent 250, 268 (29 July 1926).
26. S. F. Hou, "Lighting system with an adjustable illuminated area," U.S. patent 7,845,834 B2 (7 December 2010).
27. H. J. Birchall, "Lenses and their combination and arrangement in various instruments and apparatus," U.S. patent 2,001,952 (21 May 1935).
28. A. W. Lohmann, "A New Class of Varifocal Lenses," Appl. Opt. **9**(7), 1669–1671 (1970).
29. E. Acosta and J. Sasian, "Micro-Alvarez lenses for a tunable-dynamic-range Shack–Hartmann wavefront sensor," Jpn. J. Appl. Phys. **53**(8S2), 08MG04 (2014).
30. P. J. Smilie and T. J. Suleski, "Variable-diameter refractive beam shaping with freeform optical surfaces," Opt. Lett. **36**(21), 4170–4172 (2011).
31. T. J. Suleski, J. A. Shultz, and P. J. Smilie, "Design of Dynamic Freeform Optics," in *Renewable Energy and the Enviroment*, (Optical publishing group, 2013), paper FW2B.2.
32. T. J. Suleski, J. A. Shultz, and P. J. Smilie, "Dynamic beam shaping with freeform optics," Proc. SPIE **9194**, 91940K (2014).
33. T. J. Suleski, P. J. Smilie, and J. A. Shultz, "Dynamic laser beam shaping methods and systems," U.S. patent 9,238,577 B2 (19 January 2016).
34. R. Wu, Z. Feng, Z. Zheng, R. Liang, P. Benítez, J. C. Miñano, and F. Duerr, "Design of Freeform Illumination Optics," Laser Photonics Rev. **12**(7), 1700310 (2018).
35. Y. Ding, X. Liu, Z. Zheng, and P. Gu, "Freeform LED lens for uniform illumination," Opt. Express **16**(17), 12958–12966 (2008).

Optics EXPRESS

36. F. R. Fournier, W. J. Cassarly, and J. P. Rolland, "Designing freeform reflectors for extended sources," Proc. SPIE **7423**, 742302 (2009).
37. Z. Zhenrong, H. Xiang, and L. Xu, "Freeform surface lens for LED uniform illumination," Appl. Opt. **48**(35), 6627–6634 (2009).
38. J. J. Chen, T. Y. Wang, K. L. Huang, T. S. Liu, M. D. Tsai, and C. T. Lin, "Freeform lens design for LED collimating illumination," Opt. Express **20**(10), 10984–10995 (2012).
39. R. Hu, Z. Gan, X. Luo, H. Zheng, and S. Liu, "Design of double freeform-surface lens for LED uniform illumination with minimum Fresnel losses," Optik **124**(19), 3895–3897 (2013).
40. R. Wu, P. Liu, Y. Zhang, Z. Zheng, H. Li, and X. Liu, "A mathematical model of the single freeform surface design for collimated beam shaping," Opt. Express **21**(18), 20974–20989 (2013).
41. X. Mao, H. Li, Y. Han, and Y. Luo, "Two-step design method for highly compact three-dimensional freeform optical system for LED surface light source," Opt. Express **22**(S6), A1491–A1506 (2014).
42. D. Ma, Z. Feng, and R. Liang, "Tailoring freeform illumination optics in a double-pole coordinate system," Appl. Opt. **54**(9), 2395–2399 (2015).
43. X. Hui, J. Liu, Y. Wan, and H. Lin, "Realization of uniform and collimated light distribution in a single freeform-Fresnel double surface LED lens," Appl. Opt. **56**(15), 4561–4565 (2017).
44. P. Benítez, R. M. Arroyo, and J. C. Miñano, "Design in 3D geometry with the simultaneous multiple surface design method of nonimaging optics," Proc. SPIE **3781**, 12–21 (1999).
45. J. C. Miñano, P. Benítez, and J. Blen, "High-efficiency free-form condenser overcoming rotational symmetry limitations," Opt. Express **16**(25), 20193–20205 (2008).
46. F. Chen, S. Liu, K. Wang, Z. Liu, and X. Luo, "Free-form lenses for high illumination quality light-emitting diode MR16 lamps," Opt. Eng. **48**(12), 123002 (2009).
47. J. Y. Cai, Y. C. Lo, and C. C. Sun, "Optical design of the focal adjustable flashlight based on a power white-LED," Proc. SPIE **8128**, 812806 (2011).
48. E. Juntunen, P. Myöhänen, E. Tetri, O. Tapaninen, J. Ojalehto, and V. Heikkinen, "Rapid prototyping of freeform optics for an LED downlighter with a dynamically adjustable beam," Light Res. Technol. **48**(7), 885–897 (2016).
49. J. A. Shultz, "Design, tolerancing, and experimental characterization of dynamic freeform optical systems," Ph.D. dissertation (The University of North Carolina at Charlotte, 2017).
50. T. A. Driscoll and R. J. Braun, *Fundamental of Numerical computation* (SIAM, 2017), Chap. 5.